

Is Arcturus a well-understood K giant?

Test of model atmospheres and potential companion detection by near-infrared interferometry

T. Verhoelst^{1,3}, P. J. Bordé^{2,*}, G. Perrin³, L. Decin^{1,**}, K. Eriksson⁴, S. T. Ridgway^{3,5}, P. A. Schuller²,
W. A. Traub², R. Millan-Gabet⁵, M. G. Lacasse², and C. Waelkens¹

¹ Instituut voor Sterrenkunde, K.U. Leuven, Celestijnenlaan 200B, B-3001 Leuven, Belgium

² Harvard-Smithsonian Center for Astrophysics, 60 Garden Street, Cambridge, MA 02138, USA

³ Observatoire de Paris-Meudon, LESIA, 5 place Jules Janssen, 92195 Meudon, France

⁴ Institute for Astronomy and Space Physics, Box 515, 75120 Uppsala, Sweden

⁵ National Optical Astronomy Observatories, PO Box 26732, Tucson, AZ 85726, USA

⁶ Caltech/Michelson Science Center, Pasadena, CA 91125, USA

Received 12 November 2004 / Accepted 23 January 2005

Abstract. We present near-IR interferometric measurements of the K1.5 giant Arcturus (α Bootis), obtained at the IOTA interferometer with the FLUOR instrument, in four narrow filters with central wavelengths ranging from $2.03\ \mu\text{m}$ to $2.39\ \mu\text{m}$. These observations were expected to allow us to quantify the wavelength dependence of the diameter of a typical K giant. They are compared to predictions from both plane-parallel and spherical model atmospheres. Unexpectedly, neither can explain the observed visibilities. We show how these data suggest the presence of a companion, in accordance with the Hipparcos data on this star, and discuss this solution with respect to Arcturus' single star status.

Key words. Techniques: interferometric – Stars: individual: Arcturus – Stars: atmospheres – Stars: binaries: general

1. Introduction

Early K giants are often used as calibration sources for photometry, spectroscopy and interferometry in the (near) IR because they offer a good compromise between brightness at these wavelengths and compactness of the atmosphere. The latter quality guarantees the absence of exotic behaviour in both the line/band formation (deviations from Local Thermodynamic Equilibrium (LTE), complicated temperature distributions, ...) and in spatial structure.

One such very popular star is Arcturus (K1.5-2III, α Bootis). This star has been a stellar standard for many decades, not only in the infrared for spectroscopic/photometric work, (e.g. as an ISO-SWS calibrator, Decin et al. 2003a) but also as an IAU radial velocity standard (e.g. Pearce 1955). Although its angular diameter of about 20.20 ± 0.08 mas (Perrin et al. 1998) implies that it is too resolved by most interferometric configurations to be used as a calibrator (Sect. 2), it provides an

excellent opportunity to study the deviations from a non-wavelength-dependent uniform-disk model (which is usually used to model the calibration sources, a step necessary in the calibration process), and hence to investigate the need for sophisticated models to calibrate interferometric measurements if high-accuracy visibilities are sought. Such a detailed study of Arcturus was already performed in the visible wavelength regime by Quirrenbach et al. (1996), who found good agreement with theoretical wavelength-dependent limb-darkening predictions. In this paper, we investigate the near-IR part of the spectrum.

We start out by discussing the interferometric calibration process (Sect. 2). Then we present the data obtained on Arcturus (Sect. 3), after which we present different atmosphere models with which one can interpret the data (Sect. 4).

Surprisingly, some data points are not at all consistent with the proposed models, and seem to suggest a binary nature for Arcturus. We discuss this solution and confront it with our current knowledge of this star in Sect. 5. Finally, in Sect. 6, we summarize our results and the open questions.

* Michelson Postdoctoral Fellow

** Postdoctoral Fellow of the Fund for Scientific Research, Flanders

2. The interferometric calibration process: the need for well known calibrators

Interferometric observations measure the spatial coherence of a given source between two or more apertures. Any optical defect on the line of sight such as atmospheric turbulence or in the instrument such as polarization mismatches or dispersion will degrade spatial coherence.

The classical solution to overcome this issue of decoherence is to observe reference stars used as calibrator sources. The observed degree of coherence measured on the calibrator (also called fringe contrast) is compared to the value expected from prior knowledge of the source characteristics. This defines the interferometric efficiency (also called transfer function) of the instrument at the time when the calibrator was observed. In single-mode interferometers for which turbulent phase has been filtered out, the interferometric efficiency is relatively stable. Yet, in order to monitor any instrumental change to achieve the best accuracy, calibrator observations are interleaved with science target observations.

In an ideal world, a calibrator should be point-like in order to yield an expected visibility of 100% to within an excellent approximation. However, if we receive non-zero flux from an object then it must have a finite angular diameter. Furthermore, the requirement of IR brightness and the more or less Planckian energy distribution of stars, favours cool giants as IR interferometric calibrators. Consequently in practice, calibrators are always slightly resolved albeit with large visibilities. But an accurate visibility estimate requires an accurate diameter estimate. Some sources have been measured interferometrically or with the lunar occultation technique. But for most calibrator sources an *a priori* estimate is required. It has to be based on spectroscopy, photometry and modelling. Examples of such studies can be found in Cohen et al. (1996, 1999), Bordé et al. (2002), and Mérand et al. (2004) for the near-infrared, or Van Boekel et al. (2004) for the mid-infrared.

These indirect techniques prove to provide excellent wide-band diameter estimates with accuracies as good as a few percent, but higher spectral resolution and/or an expected visibility of the calibrator well below 100% will require a better understanding of the calibrator diameters. The observations presented here were made to empirically quantify the wavelength-dependence of the diameter of an early K giant and to test whether theoretical atmosphere models can be used to compute the wavelength-dependent diameter of other interferometric calibrators.

3. The observations

Before presenting the new data, we briefly discuss the instrument, the calibrator star and the data reduction strategy.

3.1. The instrument

The observations were performed in May 2002 at the IOTA (Infrared-Optical Telescope Array) interferometer located at the Smithsonian Institution's Whipple Observatory on Mount Hopkins, Arizona (Traub 1998). Several baselines of the IOTA have been used to sample visibilities at different spatial frequencies. The data have been acquired with FLUOR (Fiber Linked Unit for Optical Recombination) in the version described by Coudé du Foresto et al. (1998). FLUOR is the precursor of the now well-known VLT/VINCI (Kervella et al. 2000, 2003). FLUOR has four outputs (two interferometric and two photometric) which were focused on a Nicmos 3 array developed by Millan-Gabet (2000) and operated with frame rates ranging from 500 up to 2000 Hz.

Observations were carried out in narrow bands with filters specially specified for molecular bands and the continuum region of cool stars in K (e.g. Decin 2000). We will discuss in Sect. 4 which bands are present in the K band in the case of Arcturus and how they are expected to influence the interferometric observations. The narrow band filters transmissions are plotted in Fig. 2. They are named K203, K215, K222 and K239 where the three digits characterize the central wavelength: 2.03, 2.15, 2.22 and 2.39 μm respectively. The two continuum filters K215 and K222 sample the maximum transmission region of the K band. The K203 (H_2O bands) and K239 (H_2O and CO bands) sample the edges of the K band where stellar flux is attenuated by the poorer transmission of the Earth's atmosphere due to the absorption by water vapor. Any loss of coherence due to this water vapour is taken into account by measuring the interferometric efficiency in each band separately.

3.2. The calibrator star: HR 5512

Observations of Arcturus have been bracketed by observations of the calibrator star HR 5512 (M5III) whose diameter is estimated to 8.28 ± 0.41 mas as explained in Perrin et al. (1998). Using an M5 giant is of course rather risky in the sense that it probably also has a slightly extended atmosphere with a wavelength dependent diameter. And since it is partially resolved, the interferometric efficiency we used might be biased. Theoretically, one can expect an atmospheric extension of about 4–8% for a late M giant (e.g. Wittkowski et al. 2004). At a spatial frequency of 25 arcsec^{-1} , this would induce a variation with wavelength of the calibrator's visibility below 0.5%. Nevertheless, this effect must be kept in mind when interpreting the Arcturus data.

HR 5512 does not appear in the spectroscopic binary catalogues of Batten et al. (1989) and Pourbaix et al. (2004). *Hipparcos* does not list it as a visual binary either, though it does get the flag “*suspected binary*”. In response, Mason et al. (1999) used speckle interferometry to possibly resolve the system, but they found no companion.

HR 5512 is known to be a semi-regular (SR) variable star (e.g. Percy & Fleming 1992) for which *Hipparcos* found variations with an amplitude of 0.1 mag and a period of only 6.3 days (Koen & Eyer 2002). However, more recently, samples of these *Hipparcos* short-period SR's have been the subject of other dedicated photometric surveys, such as those performed by Koen et al. (2002) and Kerschbaum et al. (2001), which could not confirm the presence of any variability with a period below 35 days in any of their targets. Kerschbaum et al. (2001) suggest some instrumental artefact on the side of *Hipparcos*. We are therefore confident that the brightness of our calibrator HR 5512 has not changed significantly during the observing run. Furthermore, Koen et al. (2002) find that in most SR's, the brightness variations are primarily due to changes in temperature, and not in diameter. This suggests that the diameter variations of HR 5512 during its pulsational cycle are well below the 2% limit of the constant temperature scenario and hence do not affect our science observations.

3.3. Data reduction

Fringe contrasts have been derived with the procedure explained in Coudé du Foresto et al. (1997). The bias in visibility estimates due to photon noise has been removed following Perrin (2003a). Turbulent corrugations of the wavefront are cleaned by the single-mode fibers of FLUOR except for the differential piston between two apertures. Perrin & Ridgway (2004) have shown that the piston-induced bias is smaller than the 0.1% level for typical fringe frequencies of a few hundred Hz as used in FLUOR. The expected visibility of the calibrator is computed at the time it was observed. The interferometric efficiency is then interpolated at the time when Arcturus has been observed. Division of the fringe contrast of Arcturus by the interpolated interferometric efficiency provides the final visibility estimate. Correlations in fringe contrast and transfer function estimates are taken into account in the computation of error bars. The whole calibration procedure has been published in Perrin (2003b). The accuracy of visibility estimates measured with the FLUOR setup is usually on the order of 1% for most sources and can be as good as 0.2–0.4% (Perrin 2003b; Perrin et al. 2004a). In other words, all known biases are much smaller than the effects reported in this paper and error bars are well estimated.

Table 1 lists all measured visibilities in May 2002, grouped per filter.

4. Interpretation of the data: comparison with theoretical atmosphere models

Typical of present-day optical interferometric data is that they do not allow an inverse Fourier Transform (to obtain an image) but only offer information when they are compared to a model of the source intensity distribution on the sky. This implies that one needs to know in

Table 1. All measured squared visibilities of the 2002 run, grouped per filter. PA is the position angle (counted from North to East) of the interferometric baseline projected onto the sky.

Date (MJD)	Filter	spat. freq. (arcsec ⁻¹)	PA (deg)	V^2	$\sigma(V^2)$
52427	K203	37.70	128.44	0.1656	0.0054
52429	K203	37.27	122.93	0.1885	0.0050
52429	K203	37.32	123.35	0.1901	0.0050
52430	K203	26.68	122.37	0.4030	0.0117
52430	K203	26.69	122.63	0.3961	0.0100
52431	K203	37.62	131.03	0.1688	0.0048
52427	K215	35.01	121.57	0.2347	0.0052
52429	K215	35.25	123.75	0.2167	0.0055
52430	K215	25.18	122.97	0.4533	0.0071
52431	K215	35.46	131.41	0.2288	0.0054
52427	K222	34.02	122.02	0.2581	0.0055
52429	K222	34.25	124.28	0.2568	0.0057
52429	K222	34.30	124.74	0.2535	0.0056
52430	K222	24.44	123.38	0.5336	0.0108
52431	K222	34.36	131.70	0.2522	0.0058
52425	K239	42.09	93.42	0.0867	0.0054
52427	K239	31.08	116.61	0.2937	0.0083
52429	K239	32.00	125.74	0.2861	0.0111
52430	K239	22.74	124.06	0.5719	0.0099
52431	K239	31.94	132.04	0.2886	0.0082

advance, through previous (non-interferometric) studies, which type of model to choose. For Arcturus, a first step could be the fitting of a uniform disk model for each individual filter which yields the apparent diameters at the different wavelengths. These values can then be compared to theoretical predictions. While this strategy is satisfactory for the study of stars with very extended atmospheres for which accurate model atmospheres are not yet available and for which the observed change of size with wavelength is large, it is not sophisticated enough for Arcturus, for which we expect diameter variations with wavelength of only a few percent (Decin et al. 2003a). Hence, we would like to use a fully self-consistent theoretical model atmosphere and compute from this a wavelength-dependent, limb-darkened synthetic source intensity distribution on the sky.

4.1. Arcturus atmosphere models and diameter determination

In this section, we present our dedicated MARCS model atmospheres and the resulting spatial intensity profiles. These are then converted into synthetic visibilities and compared with the observations.

4.1.1. The atmosphere models

Arcturus was used as a primary calibrator for the calibration of the ISO-SWS (Infrared Space Observatory Short

Wavelength Spectrometer) (Decin 2000) and was for these purposes modelled using the MARCS-code (Plez et al. 1992, and references therein). This code is aimed at the modelling of atmospheres of cool (giant) stars, allowing both plane-parallel (PP) and spherical (SPH) geometries. Basic assumptions underlying the models are the following: LTE, hydrostatic equilibrium and conservation of energy for radiative and convective flux. The radiative transfer equation is solved using an ALI (Approximate Lambda Iteration) method (Nordlund 1984) with the OS (Opacity Sampling) technique as the statistical way of treating spectral lines.

Schmid-Burgk (1975) and Scholz (1985) found that the PP approximation was no longer valid in cool giants when a measure of the extension of the atmosphere, d , defined to be

$$d \equiv \frac{R_{\tau_{\text{Ross}}=10^{-5}} - R_{\tau_{\text{Ross}}=1}}{R_{\tau_{\text{Ross}}=1}} \quad (1)$$

with R the linear radius and τ_{Ross} the Rosseland optical depth, was larger than 0.05.

Recent studies of the role of sphericity in oxygen-rich cool stars include those of Scholz (1985), Bessell et al. (1989) and Plez et al. (1992). Compared to PP models, the radiation field in a SPH model becomes diluted in the upper photospheric layers. This usually leads to a decrease in temperature of the surface layers which can influence significantly the molecular opacity (Mihalas 1978, p. 650).

SPH models have to deal with the added complexity of an explicit radial dependence of all variables, plus a more complex equation of radiative transport, solved for different rays toward the observer:

$$\frac{\mu}{\kappa_{\nu}\rho} \frac{\partial I_{\nu}}{\partial r} + \frac{1-\mu^2}{\kappa_{\nu}\rho r} \frac{\partial I_{\nu}}{\partial \mu} = S_{\nu} - I_{\nu} \quad (2)$$

with $\mu = \cos\theta$ the cosine of the viewing angle, κ_{ν} the monochromatic extinction coefficient per unit mass, ρ the density, I_{ν} the specific intensity and S_{ν} the source function. Computationally, this equation is solved by using the single-ray approximation (Nordlund 1984) for a set of parallel rays, intersecting the atmosphere at different values for the impact parameter. In computer time, the difference between PP and SPH models is usually less than a factor of three although convergence is not guaranteed in the latter case.

The high quality of the fit between the resulting synthetic spectrum and both the observed ISO-SWS spectrum and high-resolution FTS spectra presented in Decin et al. (2003b), suggests that these hydrostatic models offer a good representation of the true atmosphere of Arcturus. Since this comparison was limited to the ISO-SWS wavelength region (2.38–45 μm), we searched the full Arcturus FTS spectral atlas (Hinkle et al. 1995) in the FLUOR bandpasses for peculiar spectral features. Lines are sparse (mainly CN and some atomic lines) and well spaced up to the ^{12}CO 2–0 bandhead at 2.29 μm . A comparison between the FTS spectra (summer and winter) and a spectrum synthesized from our atmosphere model

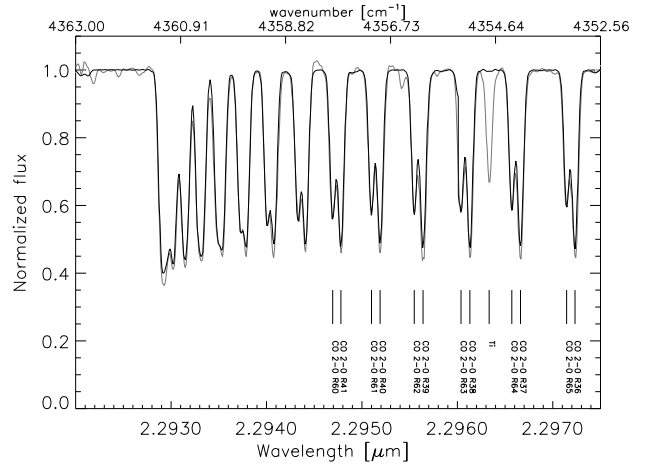


Fig. 1. FTS spectra (summer and winter, in grey) compared to our synthesized spectrum (black) at the ^{12}CO 2–0 bandhead near 2.29 μm . The good match confirms the quality of our model in the FLUOR wavelength region. The discrepancy in the Titanium line is due to a poorly known $\log gf$ value.

at this bandhead is shown in Fig. 1. Clearly the match is excellent, confirming the quality of our model.

From the quality of the fit between synthetic and observed spectra, we find little reason to prefer a SPH model over a PP one, suggesting that the atmosphere is quite compact (indeed, $d = 0.02$ for the model). Nevertheless, we computed both PP and SPH atmospheres for a grid around the stellar parameters determined by Decin et al. (2003a) for Arcturus (listed in Table 2), since the effects of sphericity may still be detectable in the intensity profile on the sky and hence also in the visibilities. From these models, we derived a spatial intensity profile for each OS wavelength point in the K band. The full OS wavelength grid of our model contains about 150,000 wavelength points, with a resolution of $R \sim 20,000$ at 2 μm . These points are chosen in such a way as to accurately sample the total opacity as a function of wavelength and is based on extensive atomic/molecular linelists and continuum opacity sources. The full K band spectrum of this model is shown in Fig. 2, together with the FLUOR filter profiles.

Table 2. The stellar parameters from Decin et al. (2003b) and references therein, and the limits of the grid in which we searched for an optimal fit to the interferometric data (ξ_t is the microturbulent velocity).

Parameter	Value	Lower limit	Upper limit
T_{eff} (K)	4320 ± 140	4250	4500
$\log g$ (cm/s^2)	1.50 ± 0.15	1.00	2.00
[Fe/H]	-0.5 ± 0.20	-1.0	0.0
ξ_t (km/s)	1.7 ± 0.3		

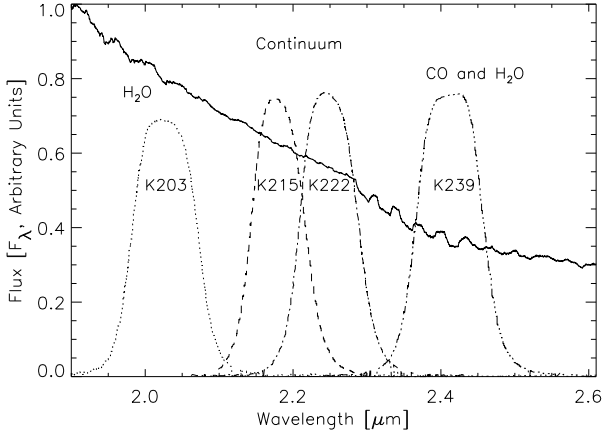


Fig. 2. The transmission curves of the 4 narrow band filters used in the FLUOR instrument on IOTA together with a synthetic K-band spectrum of Arcturus. For cool late-type stars, the filter centered at $2.03 \mu\text{m}$ probes a H_2O band in the spectrum (not present in Arcturus). For a K giant, the filters at 2.15 and $2.22 \mu\text{m}$ both probe the continuum, and the 4th filter at $2.39 \mu\text{m}$ covers the CO first overtone band (and possibly also H_2O).

The resulting variety in intensity profiles (with wavelength) is largest for the model with stellar parameters $T_{\text{eff}} = 4250 \text{ K}$ and $\log g = 1.00$ and is shown in Fig. 3 and Fig. 4. To improve display of the profile at the limb, we plot intensity as a function of $\mu = (1 - r^2/R_{\tau_{\text{Ross}}=10^{-7}}^2)^{1/2}$, where r is the projected linear distance from the center of the stellar disk. The FLUOR-bandpass-integrated profiles are overplotted in black. Even in the PP geometry there is a noticeable variety in profiles, but through the integration over the bandpasses we lose most of that information. In the SPH geometry, the variety in profiles is much stronger and even after integration differences do remain, mainly in the outer regions of the disk in the CO and H_2O probing filter¹. In this case, this is due only to CO, since the model predicts no lines of water vapor (the photospheric temperature is too high for this molecule to survive).

Because of circular symmetry, these intensity profiles can now be Hankel-transformed into visibility curves (Hanbury Brown et al. 1974)

$$V(x) = \frac{\int_0^1 I(\mu) J_0(\pi x \phi \sqrt{1 - \mu^2}) \mu d\mu}{\int_0^1 I(\mu) \mu d\mu}, \quad (3)$$

where $x = B/\lambda$ is the spatial frequency (arcsec^{-1}) with B the projected baseline and λ the wavelength, I the intensity profile, J_0 the zeroth-order Bessel function of the first

¹ We remark that high spectral resolution interferometric observations, e.g. with VLTI/AMBER (Petrov et al. 2000) will resolve the individual spectral lines visible between $\mu = 0.2$ and 0.0 . The difference in visibility curve between such a spectral line and the continuum will be much stronger than that between the different FLUOR filters discussed here.

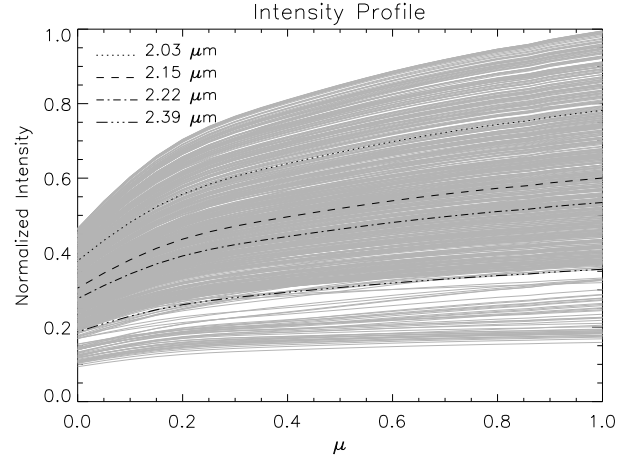


Fig. 3. Intensity profiles for a plane parallel model at $T_{\text{eff}} = 4250 \text{ K}$ and $\log g = 1.0$, normalized to the maximum intensity in the K-band at the center of the stellar disk. Every gray curve was computed for an OS wavelength within the K band. Clearly there is a wide range of shapes over the stellar disk, but integration over the bandpasses reduces the differences. Because the model is semi-infinite for all viewing angles, $\mu = 0$ corresponds to a singularity.

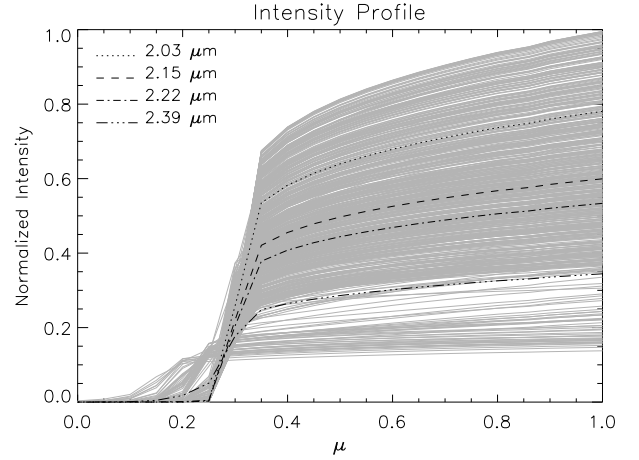


Fig. 4. Intensity profiles for a spherical model at $T_{\text{eff}} = 4250 \text{ K}$ and $\log g = 1.0$, normalized to the maximum intensity in the K-band at the center in the stellar disk. Every gray curve was computed for an OS wavelength within the K band. We now see even more variety than in Fig. 3, mainly toward the stellar limb. The $2.39 \mu\text{m}$ filter differs significantly from the others in this outer region¹.

kind, and ϕ the angular diameter. Here, the angular diameter corresponds to the image size, i.e. the outermost point of the model ($\tau_{\text{Ross}} = 10^{-7}$). It is the only free parameter of the model and is determined by fitting the theoretical curves to the observed data. The results of this fitting are presented in the next section.

4.1.2. Diameter definitions

Comparison between this image size and the different types of diameters generally used in the literature is not trivial. In the case of a uniform disk (UD), the visibility is given by

$$V(x) = \frac{2J_1(\pi x \phi)}{\pi x \phi} \quad (4)$$

with x and ϕ as in Eq. 3, and J_1 the first-order Bessel function of the first kind. Fitting a UD model to the data, we find the set of angular diameters listed in Table 3. These values are not compatible with a single wavelength-independent UD, and in addition the fit quality appears very poor in most cases (column 3 of Table 3), thus demonstrating the need for atmosphere models when precisions of $\approx 1\%$ are reached on angular diameters.

Table 3. Uniform disk (UD) angular diameters derived by fitting Eq. 4 to the narrow-band data taken in respective filters or altogether. The third column gives the reduced chi-square of the fit (chi-square per degree of freedom), denoted χ_r^2 .

filter	ϕ (UD, mas)	χ_r^2
K203	20.77 ± 0.18	9.20
K215	20.91 ± 0.15	8.26
K222	20.44 ± 0.16	0.40
K239	21.12 ± 0.25	2.01
all	20.72 ± 0.16	6.14

Alternatively, one may be interested in the limb-darkened (LD) diameter. This diameter is the actual physical diameter of the star, but is only well defined for stars with a compact atmosphere (i.e. in case of a high surface gravity). Since the outermost radial point of our atmosphere model ($R_{\tau_{\text{Ross}}=10^{-7}}$) is supposed to correspond to the physical boundary of the star, the LD diameter is actually the image size (ϕ) in the case of a SPH model (cf. Eq. 3 and the definition of μ). This is not correct for the PP models because these are semi-infinite for all viewing angles (with a singularity at $\mu = 0$), therefore the value of the intensity profile at $\mu = 0$ is an extrapolation from the last calculated μ point. This last calculated μ point depends on wavelength, because different wavelengths come with different numbers of rays in the model. Figures 3 and 4 demonstrate this difference between PP and SPH models. Consequently, the image size listed in Column 2 of Table 4 does not correspond to $R_{\tau_{\text{Ross}}=10^{-7}}$ and can not be converted into a $\tau_{\text{Ross}} = 1$ diameter as is done for the SPH models below.

A physically relevant and well defined diameter is the one corresponding to the $\tau_{\text{Ross}} = 1$ layer. It can be derived from the image size (of a SPH model) if one knows the ratio of the outermost radial point in the model to the $\tau_{\text{Ross}} = 1$ diameter. This ratio is similar to what is

called the “extension of the atmosphere”, d , as defined in Eq. 1, but for the models presented here, the outermost point corresponds to $\tau_{\text{Ross}} = 10^{-7}$. This $\phi_{\tau_{\text{Ross}}=1}$ is also presented in Table 4.

Table 4. Angular diameter determinations with plane-parallel and spherical MARCS models. Only a very small improvement on the chi-square can be achieved by increasing the extension of the atmosphere of the model (SPH model with $\log g = 1.0$), and such a low surface gravity cannot be reconciled with the spectral features.

model	PP, 4250K $\log g = 1.5$	SPH, 4250K $\log g = 1.0$	SPH, 4250K $\log g = 1.5$
ϕ (mas)	21.32 ± 0.19	22.37 ± 0.19	21.84 ± 0.21
$\phi_{\tau_{\text{Ross}}=1}$	NA	21.16 ± 0.18	21.19 ± 0.20
d (Eq. 1*)	0.030	0.057	0.030
χ_r^2	5.63	5.38	5.51

* out to $\tau_{\text{Ross}} = 10^{-7}$

Figures 5 and 6 show a comparison of our theoretical visibility curves with the observed narrow-band visibilities. For the PP model (Fig. 5), all four visibility curves coincide. The best-fit angular diameter for $T_{\text{eff}} = 4250\text{K}$, $\log g = 1.50$ and $[\text{Fe}/\text{H}] = -0.50$, is $\phi = 21.32 \pm 0.19\text{mas}$. The chi-square per degree of freedom or reduced chi-square is then $\chi_r^2 = 5.63$.

For the SPH model with the same stellar parameters (Fig. 6), the filter centered within the CO band around $2.39\mu\text{m}$ shows a slightly larger star, though that is barely visible in the plot. We obtain $\phi = 21.84 \pm 0.21\text{mas}$ for $T_{\text{eff}} = 4250\text{K}$, $\log g = 1.50$, $[\text{Fe}/\text{H}] = -0.50$. However, the improvement is small since $\chi_r^2 = 5.51$ for this model. Some improvement can be achieved by reducing the surface gravity of the model (increasing the extension of the atmosphere): this leads to a significantly different visibility curve for the CO filter, but the improvement in terms of χ_r^2 is very small (cf. Table 4), and such a low surface gravity cannot be reconciled with the observed spectral features (Decin et al. 2003b).

We remark that our newly derived diameters are slightly (but significantly) larger than the LD diameters determined in K broadband (20.91 ± 0.08 , Perrin et al. 1998) and in the optical ($21.0 \pm 0.2\text{mas}$, Quirrenbach et al. 1996). The bias introduced by the use of a single calibrator is taken into account in the error determination and should thus not be responsible for this discrepancy. The diameter of Arcturus was also estimated with spectro-photometric techniques (e.g. Cohen et al. 1999; Decin et al. 2003b; Van Boekel et al. 2004), but uncertainties on those diameters are generally much larger and therefore compatible with both our results and those discussed above. The uncertainties on the distance ($11.26 \pm 0.09\text{pc}$) derived from the parallax, the surface gravity and the mass, make it impossible to ob-

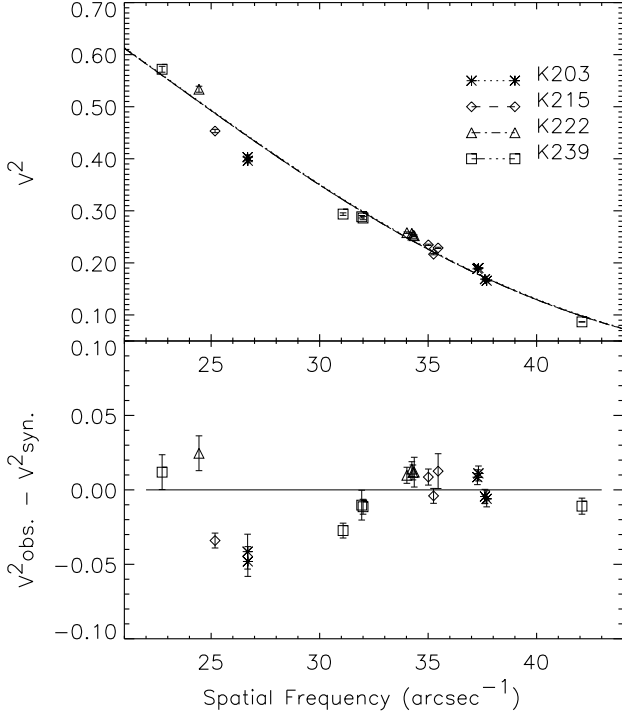


Fig. 5. A comparison between the FLUOR visibility measurements of Arcturus and a plane-parallel MARCS visibility model ($T_{\text{eff}} = 4250$ K, $\log g = 1.50$; $\chi_r^2 = 5.63$ for $\phi = 21.32 \pm 0.19$ mas). The four theoretical curves coincide, while there is a significant dispersion of the data points.

tain an accurate estimate of the angular diameter which does not depend on observed flux levels and direct (interferometric) measurements. The recently derived empirical surface brightness relation by Kervella et al. (2004) yields a diameter of 21.2 ± 0.2 (assuming a 0.02 mag error on the K magnitude) which is well in agreement with our result.

4.2. Discussion

To our surprise, neither PP nor SPH models can explain the observed visibilities. Indeed, the probability to obtain $\chi_r^2 \approx 5.6$ with 19 degrees of freedom is as low as 10^{-14} , and there appear to be systematics in the residuals. In the following, we investigate possible sources of these discrepancies.

An important characteristic of the residuals is that they not only point at a problem with the wavelength dependence of the visibility, but also at a problem with the shape of the visibility curve which is not consistent with that of a limb-darkened disk: the large discrepancy at a low spatial frequency (25 arcsec^{-1}) suggests a structure at least a few times larger than the stellar disk.

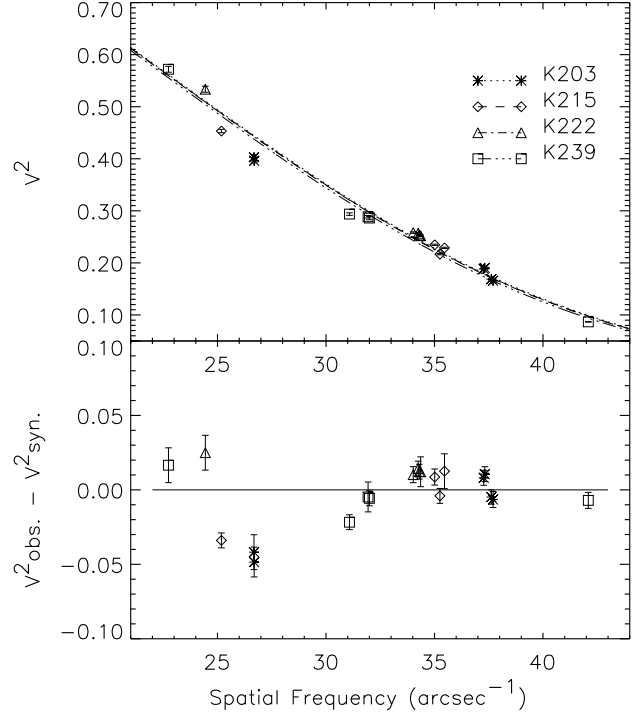


Fig. 6. For the spherical model with slightly lower surface gravity ($T_{\text{eff}} = 4250$ K, $\log g = 1.00$; $\chi_r^2 = 5.38$ for $\phi = 22.37 \pm 0.19$ mas), the visibility curve in the CO-probing filter no longer coincides with the others, corresponding to a slightly larger diameter, but it still cannot match the measured visibilities.

4.2.1. Calibration problems

A first check that needs to be done concerns the calibrator source: as discussed in Sect. 3, the extension of the calibrator's diameter should contribute at most only 0.5% to the residuals at 25 arcsec^{-1} . It is however possible that HR 5512 shows a more complicated atmosphere/circumstellar environment, but some simple calculus shows that ignoring this effect in the calibrator actually leads to an underestimation of the variation in visibility with wavelength in the science target: if the extension of the calibrator is affecting the calibration, then the problem for Arcturus is actually even larger than the few percent reported here. Only if we assume the data points that fall below the fit (e.g. those at 26 arcsec^{-1}) to be correct, can the extension of the calibrator cause the other points to be overestimated. However, these data points are not at all compatible with photometric diameter estimates of Arcturus (e.g. 20.8 mas, Decin 2000). Moreover, in such a scenario, we expect problems mostly in the wavelength dependence and not in the shape of the visibility curve.

Conclusive evidence against problems with the calibrator is provided by a limited set of similar narrow-band FLUOR data on Arcturus from a run in May 2001 (Table 5). Unlike the 2002 data presented in this paper,

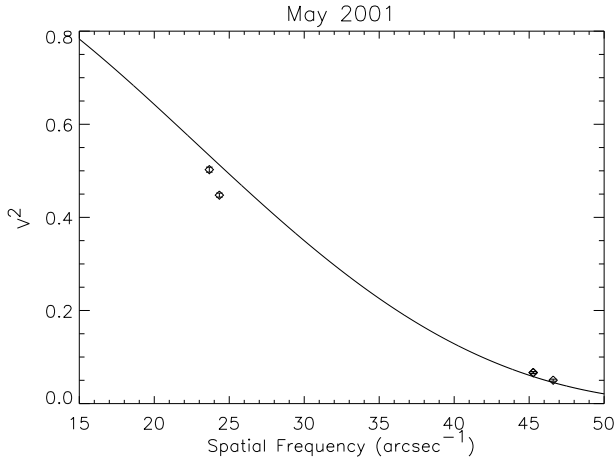


Fig. 7. Narrow-band data on Arcturus obtained in 2001 with different calibrators. The best fitting LD disk model (full line) shown here ($\chi_r^2 = 64.5$) leaves the same kind of residuals as seen in the 2002 data.

these 2001 data were calibrated with different calibrators, not including HR 5512. They are presented in Fig. 7 together with the best fit LD disk model. It is clear that these data show very similar residuals. We thus conclude that the effects reported in this paper cannot be due to the calibrator.

Table 5. All measured squared visibilities of the 2001 run, grouped per filter.

Date (MJD)	Filter	spat. freq. (arcsec ⁻¹)	PA (deg)	V^2	$\sigma(V^2)$
52043	K222	23.67	98.30	0.5079	0.0054
52047	K222	45.27	95.51	0.0684	0.0021
52043	K215	24.34	95.47	0.4522	0.0044
52045	K215	45.27	89.02	0.0689	0.0020
52047	K215	46.60	93.07	0.0525	0.0022

The largest deviations from the expected visibility were observed on only one night (MJD=52430), and one might wonder whether observing conditions showed any peculiarities that night. We found no sign of this night being any different from the others of that run. Strong piston often induces a broadening of the power spectrum of the affected fringe scans, but this is not seen in the data presented here.

4.2.2. The photosphere of Arcturus

Recently, Ryde et al. (2002) reported the presence of H₂O lines in a high-resolution Texes spectrum of Arcturus, which were not present in the MARCS model used for comparison (also used here). Ryde et al. (2002) show how the presence of these lines can be produced in the synthetic spectrum by imposing a slightly lower temperature in the

outer layers ($\log \tau_{500} \leq -4$) of the model-atmosphere. Although this new temperature distribution will influence somewhat the location of the line-forming region, the fact that the differences with the original MARCS model are only visible in a high-resolution spectrum suggest that it should not influence our low-resolution interferometric measurements.

Still, recent results on supergiant stars demonstrate that additional, non-photospheric layers of water can have such a combination of geometry and temperature that the extra absorption of stellar flux is filled in by the emission of the outer regions of the layer, leaving little trace of the significant additional water column density at medium spectroscopic resolution (e.g. Ohnaka 2004). This additional water opacity might still be detectable through individual lines in high-resolution spectra, such as the Texes spectrum and will significantly influence the interferometric observations. However, these additional water layers do create a *pseudo* continuum, affecting the spectrophotometric flux levels within the molecular bands. While this effect might still be minimal for one given band, the same temperature-geometry combination of the layer will result in a strong signature in another band. For Arcturus, Decin et al. (2003b) show that discrepancies between our MARCS model and the ISO spectrum are not present in any water band between 2.38 and 12 μ m. Moreover, the existence of non-photospheric molecular layers is generally linked to the pulsation of the central star, and is therefore unlikely in the case of Arcturus.

We might also wonder whether the pressure scale height coming out of the model is correct. It is known that this is not the case for cooler and more luminous stars (Perrin et al. 2004b). However, fitting a model with a larger atmospheric extension did not improve the χ^2 significantly (see Table 4), and the decrease in surface gravity required to obtain such an atmosphere is not compatible with spectroscopic data.

Furthermore, we must note that the dispersion seen in the FLUOR data is not only a molecular-band vs. continuum effect: the data obtained on the shortest baseline (around 25 arcsec⁻¹) show that even for the continuum filters, not all points are consistent with a limb-darkened disk geometry. This feature actually rules out the hypothesis of an under-estimation of the extension of Arcturus' atmosphere: even if more pronounced than in the SPH models, it could never influence the intensity profile in the continuum to this extent.

Another hypothesis could be the presence of spots on the stellar surface. However, this extra small scale structure would produce oscillations in the visibility curve whose period must be larger than the first null spatial frequency and hence it cannot explain our data. If we believe these data points are correct (and we see no reason not to), more exotic solutions should be explored.

We are of course aware of Arcturus' status as calibrator source for many different instruments/techniques and of the research done on this object in that framework but the following subsection will show that some further

investigation is nevertheless necessary to explain our interferometric data and, for example, also the *Hipparcos* data on Arcturus.

5. The binary hypothesis

In this section, we investigate the possibility that the discrepancy between the MARCS model and our interferometric data might be due to the presence of a faint companion. Moreover, we discuss the consistency of this hypothesis in the light of previously published works.

5.1. Binary model

Let us denote by V_1 and V_2 the visibilities of Arcturus and its companion considered as a single stars. The companion is assumed to be unresolved ($\phi_2 = 0$), therefore $V_2 = 1$, and for V_1 we use the limb-darkened model of Eq. 3. The contrast ratio between the two stars, $r \equiv F_1/F_2$ with F the received flux, is assumed to be identical for all four filters. This might be too crude an approximation if the spectral types of the two stars differ significantly, but we show in Sect. 5.2.4 that this cannot be the case. We neglect the motion of the companion during the 7 days of our observation run, so that its separation ρ and position angle θ would remain constant. The squared modulus of the visibility for the binary then reads

$$V^2 = \frac{r^2 V_1^2 + V_2^2 + 2rV_1V_2 \cos[2\pi(B/\lambda)\rho \cos(\theta - \theta_B)]}{(r+1)^2}, \quad (5)$$

where (B, θ_B) are the polar coordinates of the interferometric baseline vector projected onto the sky. Note that for this equation to be valid, the companion's fringe packet should be well overlapped with the primary star's fringe packet. Since the narrow filters used here guarantee about 55 fringes in the fringe packet, while the derived separation between the 2 components (Table 6) corresponds to only 7 fringes, Eq. 5 can be used. The parameters ρ , θ , r and ϕ_1 are estimated by minimizing a standard χ^2 with the Levenberg-Marquardt procedure. One should be particularly careful in the search for the global minimum as trigonometric functions in Eq. 5 cause the χ^2 hypersurface to have many local minima. To overcome this problem, we use a four-dimensional grid of initial guesses to run the minimization, and keep the best χ^2 of all. With this set of data, the estimation is made more difficult by the fact that the visibility curves were not sampled with the idea of looking for a binary (a continuous sampling at one wavelength would have been much more efficient).

The best solution (Table 6) has a reduced χ^2 of 2.6, twice as low as the best single-star model. For this solution, we have plotted in Fig. 8 the expected evolution of the squared visibility during our five nights on Arcturus together with the measured values. For comparison, Fig. 9 presents the same thing for the single-star SPH model. From the marginal χ_r^2 curves in Fig. 10, we see that there is no ambiguity on the global minimum with respect to r

Table 6. Best-fit parameters with formal errors for the binary model.

	This work (K band)	<i>Hipparcos</i> (V band)
ρ	212.7 ± 1.5 mas	255 ± 39 mas
θ	157.6 ± 1.7 deg	198 deg
r	50.1 ± 5.6	21.5 ± 5.9
Δm	4.25 ± 0.12	3.33 ± 0.31
ϕ_1	21.56 ± 0.05 mas	
ϕ_2	0 (fixed)	
χ_r^2	2.6	

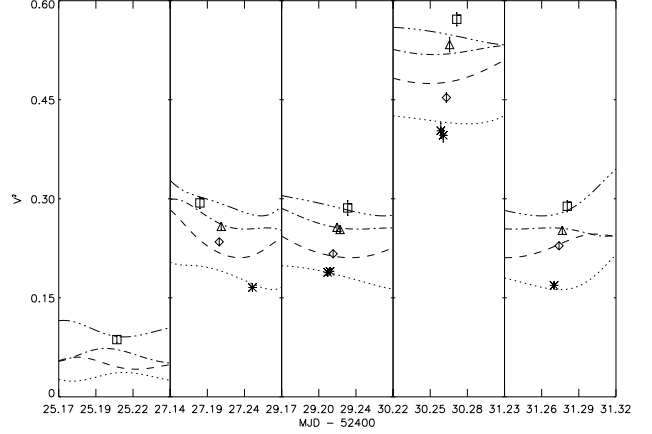


Fig. 8. Squared visibility as a function of time, and the best fitting binary model.

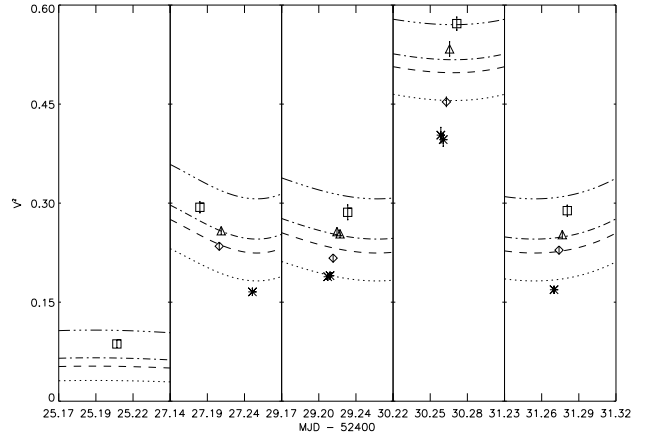


Fig. 9. Squared visibility as a function of time, and the best fitting single-star SPH model.

and ϕ_1 , the situation being more delicate for ρ and θ owing to the trigonometric functions in the model. Figures 11 and 12 show the confidence regions for the best solution as contours of the χ^2 surface in the two subspaces (ρ, θ) and (r, ϕ_1) . The form of Eq. 5 favours the correlation between the parameters in each of these pairs (98% and 57% respectively), something that can be seen from the elongated shapes of the confidence regions as well.

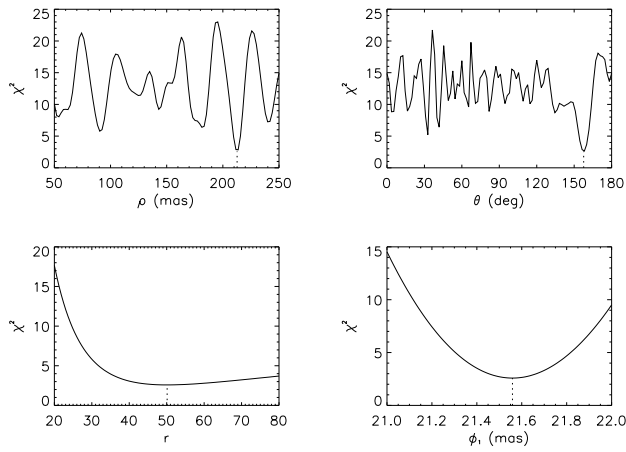


Fig. 10. Marginal χ^2 for separation ρ , position angle θ , contrast ratio r and primary angular diameter ϕ_1 . Global minima are marked by a dotted line.

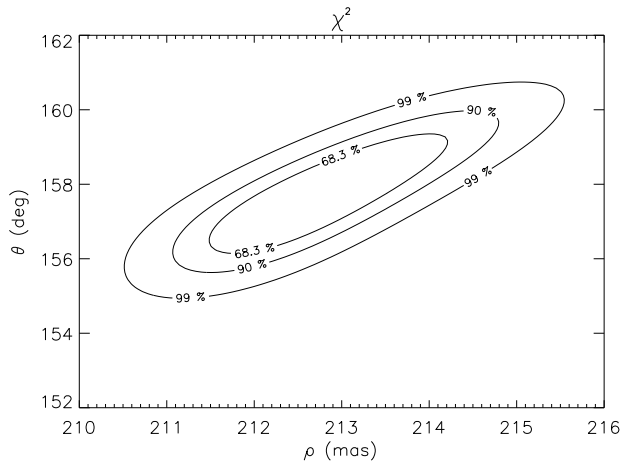


Fig. 11. Confidence intervals as a function of separation ρ and position angle θ .

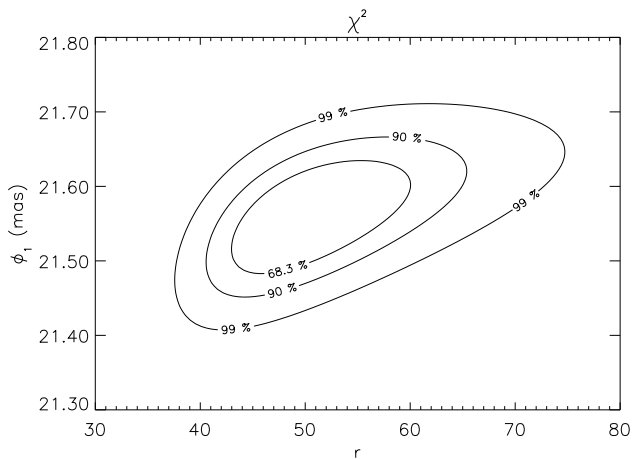


Fig. 12. Confidence intervals as a function of contrast ratio r and primary angular diameter ϕ_1 .

5.2. Discussion

Although Arcturus is generally believed to be a single star, a literature study reveals that *Hipparcos* also lists Arcturus as a double star. This result caused some debate at that time (e.g. Griffin 1998; Turner et al. 1999) and in response, the *Hipparcos* team re-analyzed the data, and – though they arrived at the same conclusion – flagged the solution as “unreliable” (Soderhjelm & Mignard 1998). Surprisingly, our solution agrees quite well with the *Hipparcos* solution (Table 6) and we are therefore convinced that this hypothesis deserves further investigation. In the following, we will first rule out the possibility of a background star and a double calibrator, then we review briefly all relevant published works on Arcturus and finally confront these with our new results.

5.2.1. Background star

As a first step, we can rule out the possibility of a visual binary, in the sense of a purely optical effect, since the high proper motion of Arcturus (-1093.43 and -1999.43 mas/yr in α resp. δ , Perryman et al. 1997) would have increased the separation with the hypothetical background star by more than $10''$ since the time of the *Hipparcos* observations, clearly separating the fringe packets of both stars. Furthermore, we obtained a new optical image of Arcturus and its neighborhood using the new CCD camera MEROPE on the 1.2 m Belgian Mercator telescope (<http://www.mercator.iac.es/instruments>). Images were made in all filters of the Geneva system (e.g. Rufener & Nicolet 1988) but only in the (narrow) U band and with an exposure time below 0.01 s did the flux not reach the saturation limit of the camera. This image confirmed that no other star of sufficient magnitude is present at Arcturus’ location in May 2002 (about $5''$ north-east from its current location) and at the time of the *Hipparcos* observations.

5.2.2. Binary calibrator

If the calibrator HR 5512 were a close binary with a sufficiently bright companion, using a UD model to compute the interferometric efficiency might introduce the calibrator binary signature into the science observations. However, in Sect. 3 we already argued that HR 5512 is not a known binary and in Sect. 4.2 we showed how fitting the 2001 data set (for which other calibrator stars were used) with a LD model yielded similar residuals, resulting in a $\chi_r^2 = 64.5$. We are therefore confident that the effects reported here are not due to binarity of the calibrator.

Fitting a binary model to this 2001 dataset on Arcturus is possible, and returns parameters roughly consistent with those determined from the 2002 dataset: a separation of 188.5 ± 5.3 mas and a magnitude difference of 3.8 mag. The resulting χ_r^2 of 1.65 is a clear improvement over the LD disk model. We must remark that the 2001

position angle (PA = 78°) differs significantly from that of 2002, but with such a limited dataset, this result is not very meaningful.

5.2.3. The literature

Radial velocities: The radial velocity of Arcturus has been studied for over a century now (e.g. Lord 1904) and, because of the stability of its velocity, has more recently become an IAU radial velocity standard (Pearce 1955).

Nevertheless, velocity variations on several time-scales have been reported in the last decades. Irwin et al. (1989) obtained precise measurements of the radial velocity on 43 occasions between 1981 and 1985. These show a range of 500 m/s, with both short-period and long-period variability. For the long-period variability, they find an amplitude of 120 to 190 m/s and a period of 640–690 days. Since this period is longer than the fundamental radial mode of oscillation, they discuss other possibilities: convection cells and dark spot are not really compatible with the absence of line-width changes. A companion with an $M \sin i$ of 1.5 to 7.0 Jupiter masses could explain their data. Explaining the long-period variability with beating of higher frequencies did not work well. In the last decade, a mode of pulsation with an even longer period has been discovered: the gravity-mode. However, the periods associated with the g-mode are still well below 2 years, and it is not certain that these pulsations are observable through an extended giant atmosphere (Mazumdar, private communication).

Although he does not present a detailed analysis of his data in this context, Cochran (1988) also notes a long period variability in his observations. Note that solar-like oscillations have recently been observed in Arcturus (Merline 1996; Retter et al. 2003).

Astrometry: No astrometric evidence for binarity was found by *Hipparcos* during its 4 year lifetime. However, Gontcharov et al. (2001) combined astrometric ground-based catalogues containing epochs later than 1939 and the *Hipparcos* catalogue, to obtain new proper motions and to detect non-linear astrometric behaviour. In their catalogue (“Proper Motions of Fundamental Stars”), Arcturus is listed as being an astrometric binary. Gontcharov (private communication) confirmed that the astrometric offsets (the residuals after subtraction of all linear motions) are significantly higher than what can be expected for a single star system. Periods of 5 and 20 years appear to be present in these data.

Direct evidence: The only other direct evidence is the visual detection of a companion by *Hipparcos*. The published results are listed in Table 6. Originally, no relative motion of the system was detected during the *Hipparcos* lifetime. However, after re-analysis of the data, a small relative motion of $4\text{--}8''/\text{yr}$ was detected, though at a PA which is “almost at right angles” with the published value (Soderhjelm & Mignard 1998).

All other attempts at a direct detection of a companion around Arcturus have returned no positive results. These include the non-detection in the H α filter with the AO system on the Mount Wilson 100 Inch Telescope by Turner et al. (1999). However, looking at Fig. 1 of this paper, a companion at a 255 mas separation would be located on the 2.0×10^3 contour of the primary’s Point Spread Function (PSF). Assuming that the PSF peaks at 3.0×10^4 at least, a contrast ratio of 20, i.e. 1.5×10^3 at most, would be below the level of the PSF, making the detection difficult. Moreover, the reconstructed image is not diffraction-limited (as 65 mas would be the size of the first Airy ring), and not circularly-symmetric, showing that residual aberrations are present. Now speckle noise is certainly a concern for faint companion detection, so we believe these observations cannot definitely rule out the companion as found by *Hipparcos*.

Nevertheless, another non-detection with Keck aperture masking, and the (apparent) absence of another fringe packet in IOTA/IONIC (broadband) H-band interferometric observations (Monnier, private communication) suggest Arcturus to be a single star indeed. Unfortunately, these data/results were not conclusive (Monnier, private communication). Quirrenbach et al. (1996) found a good agreement between their optical interferometric data on Arcturus and theoretical limb-darkening profiles. Especially the very low visibility measured around the first null (their Fig. 3c) seems incompatible with an unresolved companion only 25 times fainter than Arcturus.

Spectrophotometric observations It is noteworthy here that recent NLTE atmospheric modelling and spectrum synthesis calculations have been unable to match the observed spectrophotometric data in the violet and near UV bands: the flux observed between 300 and 400 nm amounts to only half of the predicted flux (Short & Hauschildt 2003). While this unresolved discrepancy might have nothing to do with binarity, it is a further clue that there may be more to Arcturus than is known.

5.2.4. Nature of the companion

According to our binary model (Table 6), the contrast ratio primary/companion in the K band amounts to about 50. The UV problem mentioned in Sect. 5.2.3 not taken into account, there is no clear photometric evidence of a composite SED/spectrum (Fig. 13). Therefore, the companion should emit as an object of fairly similar spectral type: if it were significantly warmer, the contrast ratio in the optical would be much lower, resulting in a clearly composite SED. If the companion were cooler (but coeval), it would have to be a giant further in its evolution and thus more massive and brighter than the primary². This is clearly not a possibility. We can therefore conclude

² Note that a Brown Dwarf is not a possibility for it would not reach the required brightness (4 mag) in the K band as derived from the contrast ratio r .

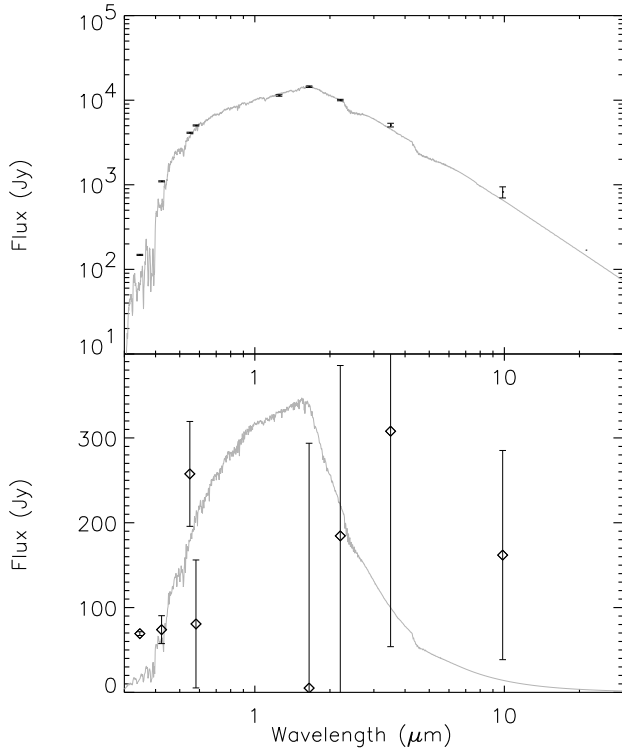


Fig. 13. Upper panel: Comparison of new UBVG (Geneva), JHKL (SAAO) and IRAS fluxes with a synthetic SED computed from our MARCS model atmosphere for Arcturus (A). There is no clear indication of a composite SED. Lower panel: the companion we suggest here (Kurucz model shown), would not be detectable in the residuals after subtraction of the primary.

that this contrast ratio is a good upper limit on the luminosity ratio of the two stars. In case of a slightly warmer companion, the luminosity ratio could possibly be a factor of two lower, i.e. 25. Adopting a total luminosity of $196(\pm 21)L_{\odot}$ as determined by Decin (2000), and a luminosity ratio range of 25–50, the primary would contribute 188–192 L_{\odot} and the companion 4–8 L_{\odot} .

A companion of similar spectral type and 4–8 L_{\odot} can only be a red (sub-)giant of slightly lower initial mass than Arcturus. Note that a higher mass is not possible because of evolutionary reasons: in such case, the companion would have been much brighter than the primary, under the assumption that they are coeval.

A quantitative estimate of the allowed mass ratio and spectral types can be made using synthetic isochrones/evolutionary tracks. Using the Padova database of stellar evolutionary tracks (Girardi et al. 2000) for $z = 0.004$, and the luminosity, T_{eff} and $\log g$ of Decin (2000), we find for the primary (and the possible system) an age range from about $10^{9.85}$ to $10^{10.25}$ years (7 to 17 billion years, actually limited by the age of the universe). In Fig. 14, we present luminosity as a function

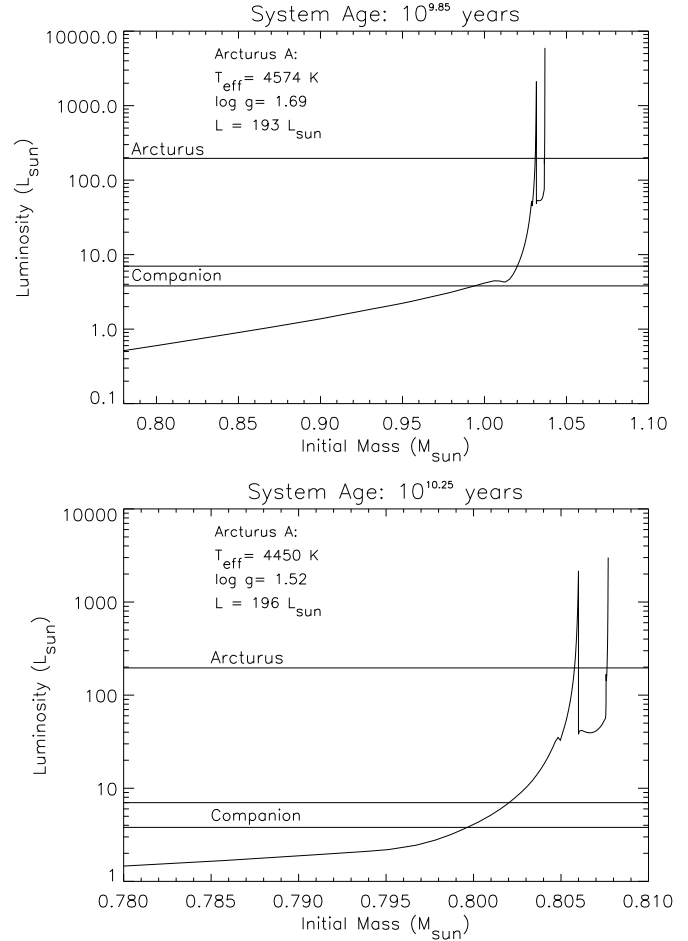


Fig. 14. Luminosity as a function of initial mass for a system of $10^{9.85}$ and $10^{10.25}$ years old. For the companion, we indicate the possible range in luminosity. The two peaks in luminosity on the right hand side correspond to the RGB and AGB phase respectively.

of initial mass for the lower and upper limit on the age of the system.

Table 7. Primary and companion stellar parameters for age-limits².

Log(Age)	9.85		10.25	
	A	B	A	B
L (L_{\odot})	195	3.8–8	195	3.8–8
T_{eff} (K)	4574	5050–6300	4450	4950–5050
$\log g$	1.69	3.5–4	1.52	3.5
M_{initial}	1.03	0.99–1.02	0.805	0.799–0.802
M_{actual}	1.02	0.99–1.01	0.796	0.796
Spect. Type	K0III	G5IV–F7IV	K1.5III	G5IV

In Table 7, we present the stellar parameters for primary and companion at the two edges of the age interval³. From this table, it is clear that the stellar parameters determined by Decin (2000) correspond to a fairly old system, but the values found for the 7-billion-year system are still compatible with the literature on α Bootis. Note that the lower mass in the “old” solution corresponds to the mass estimate implied by the measured radius and the derived gravity, which is close to $0.8 M_{\odot}$. Furthermore, the V–K colour (1.98) one obtains for the companion when combining our K-band solution with the *Hipparcos* V-band solution corresponds to a spectral type of G4IV (e.g. Bessell et al. 1998), exactly what can be expected from Table 7 and our preference for a high-age solution! To obtain a K-band contrast of 50, the companion would need to be about 2.7 mas large. This value is entirely compatible with the evolutionary model of the companion put at a distance of 11.26 ± 0.09 pc (derived from the parallax) and with the diameter computed with the empirical surface brightness relation from Kervella et al. (2004), which yields 2.72 ± 0.04 . It is compatible as well with the binary parameters reported in Table 6, as recomputing the binary model with $\phi_2 = 2.7$ mas does not lead to a noticeable change in the solution.

In the lower panel of Fig. 13, we present the absolute flux of this hypothetical companion together with the residuals we obtain by subtracting a model for the primary from the observed photometry⁴. Clearly, the companion would not be detectable in these residuals, except maybe for the B and V bands (U should be treated with much care because it is highly surface-gravity sensitive), which show significant excess, compatible with the suggested 2.7-mas G4IV companion.

Note that we found the current secondary mass to be almost equal to the primary mass. A mass ratio so close to unity, unlikely as it seems, is compatible with statistical binary mass ratio studies showing a bimodal distribution with one peak toward a ratio of 1 (e.g. Trimble 1974). The difference in luminosity is the result of the companion being slightly behind in evolution.

5.2.5. The orbit

Combining all of these results, two plausible types of orbit remain: (1) a very narrow system (separation of just a few AU) seen face-on or (2) a very wide system (period of the order of centuries, or larger) seen nearly edge-on.

The first solution does require us to discard the PA/relative motion detected in the *Hipparcos* data,

³ The actual T_{eff} determined by Decin (2000) is beyond the grid-limit, but by extrapolation one can see that this probably does not influence our results.

⁴ The diameter of the primary was chosen in such a way as to obtain positive residuals (except for the J-band which is notoriously sensitive to the water column density in the earth’s atmosphere). This required a slightly smaller diameter than derived in Sect. 4.1.2, i.e. 20.0 mas.

which is acceptable given the doubts expressed by Soderhjelm & Mignard (1998) in the re-analysis of the data. It would however be compatible with the periods found in radial velocities and astrometry of the order of a few years. To explain the low observed radial velocity variations, the inclination must be very close to face-on, or the companion must have a mass of just a few Jupiter masses, which is not compatible with the observed luminosity.

The second solution would require a nearly edge-on disk to produce the small projected separation, and the long orbital period would explain the non-detection of high-amplitude radial velocity and astrometric variability. Clearly, it is not possible to combine all results into one consistent explanation.

6. Conclusions and Outlook

We have presented a new set of narrow-band near-IR interferometric observations of the K2 giant Arcturus, obtained to test the applicability of K giants and K giant models to the calibration of high-accuracy infrared interferometric observations. A comparison with state-of-the-art stellar atmospheres failed to explain the data: the residuals show clear systematics. These are independent of calibration and none of our hypotheses about the stellar atmosphere (extension, spots) can explain the data. A binary model, with a sub-giant as companion, does provide a good fit to the data. A thorough literature study reveals that there is ample, but inconclusive and inconsistent evidence for a companion.

6.1. Implications on calibration

If the calibrator one uses is an unknown binary, or the effects reported in this paper are due to some other unknown characteristics of K giant stars, then the error on the visibility could be increased by a factor as large as $\sqrt{\chi_r^2} = \sqrt{5.6} \approx 2.5$, if a standard model atmosphere is used to represent the calibrator. For single-mode interferometers such as FLUOR or VINCI, it means that the standard error on the visibility would jump from 1–2% to 2.5–5%. Further investigation is urgently required to settle this major issue. This should include both new observations of other “normal” K giants to check the uniqueness of the problems reported here, and the re-observation of Arcturus to pin-point with more certitude the nature of this star.

6.2. Prospects for Arcturus

Unfortunately, our dataset which was aimed at determining the wavelength dependence of the diameter of Arcturus (A), does not allow a full characterization of the (still hypothetical) system. New attempts at imaging with the most recent AO systems might resolve the system, though the brightness of the primary will seriously complicate the observations. Another possibility would be

a new interferometric dataset with two telescopes on similar or shorter baselines, but obtained over a wide range of azimuth angles, such that the companion would pass through several of the fringes, providing a much clearer signal than was possible with the present essentially snapshot data set. Yet another possibility would be an interferometric data set with three telescopes (e.g. the present IOTA), using two short baselines to lock on the fringes, and one long baseline on which the large-diameter primary would have weak fringes but the small-diameter secondary would have relatively strong fringes, again observing over a large range of position angles so that the secondary passes through many fringes, for a clear signature.

Acknowledgements. The authors would like to thank John Monnier for his search of a faint companion in his Keck aperture masking and IOTA/IONIC observations of Arcturus, as well as Guillermo Torres for his valuable comments on a draft of this paper and the referee, dr. Ian Short, for his critical reading and suggestions. T.V. appreciated support by the European Community through a Marie Curie Training Fellowship for an extended stay at Paris-Meudon Observatory. (The European Community is not responsible for the information communicated.) This work was also performed in part under contract with the Jet Propulsion Laboratory (JPL) funded by NASA through the Michelson Fellowship Program. JPL is managed for NASA by the California Institute of Technology.

References

- Batten, A. H., Fletcher, J. M., & MacCarthy, D. G. 1989, *Publications of the Dominion Astrophysical Observatory Victoria*, 17, 1
- Bessell, M. S., Brett, J. M., Wood, P. R., & Scholz, M. 1989, *A&A*, 213, 209
- Bessell, M. S., Castelli, F., & Plez, B. 1998, *A&A*, 333, 231
- Bordé, P., Coudé du Foresto, V., Chagnon, G., & Perrin, G. 2002, *A&A*, 393, 183
- Cochran, W. D. 1988, *ApJ*, 334, 349
- Cohen, M., Walker, R. G., Carter, B., et al. 1999, *AJ*, 117, 1864
- Cohen, M., Witteborn, F. C., Carbon, D. F., et al. 1996, *AJ*, 112, 2274
- Coudé du Foresto, V., Perrin, G., Mariotti, J., Lacasse, M., & Traub, W. 1997, in *Integrated Optics for Astronomical Interferometry*, 115–125
- Coudé du Foresto, V., Perrin, G., Ruilier, C., et al. 1998, in *Proc. SPIE Vol. 3350*, p. 856–863, *Astronomical Interferometry*, Robert D. Reasenberg; Ed., 856–863
- Decin, L. 2000, PhD thesis, University of Leuven
- Decin, L., Vandebussche, B., Waelkens, C., et al. 2003a, *A&A*, 400, 709
- . 2003b, *A&A*, 400, 679
- Girardi, L., Bressan, A., Bertelli, G., & Chiosi, C. 2000, *A&AS*, 141, 371
- Gontcharov, G. A., Andronova, A. A., Titov, O. A., & Kornilov, E. V. 2001, *A&A*, 365, 222
- Griffin, R. F. 1998, *The Observatory*, 118, 299
- Hanbury Brown, R., Davis, J., & Allen, L. R. 1974, *MNRAS*, 167, 121
- Hinkle, K., Wallace, L., & Livingston, W. 1995, *PASP*, 107, 1042
- Irwin, A. W., Campbell, B., Morbey, C. L., Walker, G. A. H., & Yang, S. 1989, *PASP*, 101, 147
- Kerschbaum, F., Lebzelter, T., & Lazaro, C. 2001, *A&A*, 375, 527
- Kervella, P., Coudé du Foresto, V., Glindemann, A., & Hofmann, R. 2000, in *Proc. SPIE Vol. 4006*, p. 31–42, *Interferometry in Optical Astronomy*, Pierre J. Lena; Andreas Quirrenbach; Eds., 31–42
- Kervella, P., Gitton, P. B., Segransan, D., et al. 2003, in *Interferometry for Optical Astronomy II*. Edited by Wesley A. Traub. *Proceedings of the SPIE*, Volume 4838, pp. 858–869 (2003)., 858–869
- Kervella, P., Thévenin, F., Di Folco, E., & Ségransan, D. 2004, *A&A*, 426, 297
- Koen, C. & Eyer, L. 2002, *MNRAS*, 331, 45
- Koen, C., Laney, D., & van Wyk, F. 2002, *MNRAS*, 335, 223
- Lord, H. C. 1904, *ApJ*, 19, 246
- Mérand, A., Bordé, P., & Coudé du Foresto, V. 2004, *A&A*, submitted
- Mason, B. D., Martin, C., Hartkopf, W. I., et al. 1999, *AJ*, 117, 1890
- Merline, W. J. 1996, *Bulletin of the American Astronomical Society*, 28, 860
- Mihalas, D. 1978, *Stellar atmospheres*, 2nd edn. (San Francisco: W. H. Freeman and Co.)
- Millan-Gabet, R. 2000, PhD thesis
- Nordlund, A. 1984, in *Methods in Radiative Transfer*, 211–233
- Ohnaka, K. 2004, *A&A*, 421, 1149
- Pearce, J. 1955, *Trans. IAU*, 9, 441
- Percy, J. R. & Fleming, D. E. B. 1992, *PASP*, 104, 96
- Perrin, G. 2003a, *A&A*, 398, 385
- . 2003b, *A&A*, 400, 1173
- Perrin, G., Coudé Du Foresto, V., Ridgway, S. T., et al. 1998, *A&A*, 331, 619
- Perrin, G. & Ridgway, S. T. 2004, *A&A*, submitted
- Perrin, G., Ridgway, S. T., Coudé du Foresto, V., et al. 2004a, *A&A*, 418, 675
- Perrin, G., Ridgway, S. T., Mennesson, B., et al. 2004b, *A&A*, 426, 279
- Perryman, M. A. C., Lindegren, L., Kovalevsky, J., et al. 1997, *A&A*, 323, L49
- Petrov, R. G., Malbet, F., Richichi, A., et al. 2000, in *Proc. SPIE Vol. 4006*, p. 68–79, *Interferometry in Optical Astronomy*, Pierre J. Lena; Andreas Quirrenbach; Eds., 68–79
- Plez, B., Brett, J. M., & Nordlund, Å. 1992, *A&A*, 256, 551
- Pourbaix, D., Tokovinin, A. A., Batten, A. H., et al. 2004, *A&A*, 424, 727
- Quirrenbach, A., Mozurkewich, D., Buscher, D. F., Hummel, C. A., & Armstrong, J. T. 1996, *A&A*, 312, 160

- Retter, A., Bedding, T. R., Buzasi, D. L., Kjeldsen, H., & Kiss, L. L. 2003, *ApJ*, 591, L151
- Rufener, F. & Nicolet, B. 1988, *A&A*, 206, 357
- Ryde, N., Lambert, D. L., Richter, M. J., & Lacy, J. H. 2002, *ApJ*, 580, 447
- Schmid-Burgk, J. 1975, *A&A*, 40, 249
- Scholz, M. 1985, *A&A*, 145, 251
- Short, C. I. & Hauschildt, P. H. 2003, *ApJ*, 596, 501
- Soderhjelm, S. & Mignard, F. 1998, *The Observatory*, 118, 365
- Traub, W. A. 1998, in *Proc. SPIE Vol. 3350*, p. 848-855, *Astronomical Interferometry*, Robert D. Reasenberg; Ed., 848-855
- Trimble, V. 1974, *AJ*, 79, 967
- Turner, N. H., Ten Brummelaar, T. A., & Mason, B. D. 1999, *PASP*, 111, 556
- Van Boekel, R., Verhoelst, T., Leinert, C., et al. 2004, *A&A*, submitted
- Wittkowski, M., Aufdenberg, J. P., & Kervella, P. 2004, *A&A*, 413, 711